

Tuning Guidelines for Generalized Notch Filters used for Unbalance Compensation for Magnetic Bearings

Michael HUBATKA*, Beat AESCHLIMANN*

* Mecos AG, Industriestrasse 26, 8404 Winterthur, Switzerland, michael.hubatka@mecos.com

Abstract—Unbalance compensation in magnetic bearing control algorithms are state of the art in modern applications of active magnetic bearings. The compensation is vital to keep synchronous vibrations on the housing on a minimum level and to avoid actuator saturation.

There exist different possibilities to implement the compensation in the control loop. One of it is the generalized notch filter [1]. This filter technology has been successfully used in magnetic bearings for more than 20 years.

One drawback of this filter is the speed dependent parameter set. For radial bearings of a five axis rotor, the notch filter parameters are in general two dense 4x4 matrices for one rotational speed. This high demand on computational power and memory is not a problem any more for modern digital signal processors. With a well tuned parameter set the unbalance compensation can be turned on well before crossing the rigid body modes.

The paper presents a novel observer based stability proof of the generalized notch filter and introduces two bode diagrams to visualize the notch filter performance and robustness. The results are verified with a simple example and on a small 5-axis test rotor system.

I. INTRODUCTION

This paper presents a novel observer based approach to formulate the stability proof of the generalized notch filter. A time dependent state space description and a time dependent similarity transformation is used to convert the description into a linear time invariant system, allowing standard observer theory [2] to formulate the observer equations.

It has been shown in [1] that this filter is added to the nominal control loop as an additional feedback like in classical cascade control techniques. This gives the benefit of independent tuning of the nominal position controller (the inner loop) for robust stabilization and the notch filter (outer loop). This kind of implementation makes it also possible to switch the filter on and off very easily without compromising the stability of the inner loop.

The internal states of the filter can be used to calculate the magnitude and the angle of the unbalance response. This information can be used to calculate compensation weights for rotor balancing, to supervise the unbalance or even to apply some counteracting control [3].

The generalized notch filter has also good numerical properties. It is possible to implement very narrow notch filters with very lightly or even undamped poles. The undamped case is

achieved by setting the observer gains to zero (the filter is "frozen"). The adaption is turned off but because the internal states are not zero, the filter output is a harmonic oscillation.

The first part of the paper contains an observer based stability proof. It forms the basis to select an appropriate parameter set. It is also used to evaluate the properties of the filter when the parameter set is given or simplified due to implementation constraints.

The main part of the paper shows how the calculated notch filter parameters are used to estimate the performance and the robustness of the filter. For this purpose a novel bode diagram is introduced to visualize the difference between the desired and the achieved locations of the notch filter poles. This graph helps to select the speed ranges at which the filter is switched on.

This novel bode diagram is only valid when the notch filter poles are far enough away from other poles of the closed loop system with respect to the notch filter zeros. This condition is violated near the rigid body and flexible modes. For this reason an additional diagram with a stability radius is introduced that visualizes the stability margin. In frequency ranges where the rigid body or flexible modes are close, the margins can become significantly smaller. The paper suggests methods to improve robustness in these regions by changing the optimal pole locations.

In the last part of the paper the notch filter performance and robustness is evaluated in an example and on a small test rotor system. It is shown that the predicted filter properties match with the measured system responses.

Additionally, the paper outlines some aspects for the discrete implementation and simulation of the notch filter.

II. OBSERVER BASED STABILITY PROOF

The unbalance response is modelled as a sinusoidal disturbance vector $d(t)$ which is part of the measured signal $y(t)$. The notch filter has to remove the disturbance $d(t)$ from the measured signal. This is achieved by modelling the disturbance as the impulse response of a linear system and to apply the theory of an observer to estimate the unbalance.

The signal of a sinusoidal disturbance is defined as

$$\begin{aligned} \mathbf{d}(t) &= \mathbf{a}_1(t) \sin(\Omega t) + \mathbf{a}_2(t) \cos(\Omega t) \\ &= \begin{bmatrix} \sin(\Omega t) \mathbf{I} & \cos(\Omega t) \mathbf{I} \end{bmatrix} \begin{bmatrix} \mathbf{a}_1(t) \\ \mathbf{a}_2(t) \end{bmatrix} \end{aligned} \quad (1)$$

where Ω is the rotational frequency in radians per second and $\mathbf{a}_1(t)$, $\mathbf{a}_2(t)$ are the amplitudes of the sine and cosine. To convert this signal to a linear model, it is assumed that the amplitudes $\mathbf{a}_1(t)$ and $\mathbf{a}_2(t)$ are constant

$$\begin{aligned} \dot{\mathbf{a}}_1(t) &= \mathbf{0} \\ \dot{\mathbf{a}}_2(t) &= \mathbf{0}. \end{aligned}$$

The state space description is

$$\begin{aligned} \begin{bmatrix} \dot{\mathbf{a}}_1(t) \\ \dot{\mathbf{a}}_2(t) \end{bmatrix} &= \begin{bmatrix} \mathbf{0} & \mathbf{0} \\ \mathbf{0} & \mathbf{0} \end{bmatrix} \begin{bmatrix} \mathbf{a}_1(t) \\ \mathbf{a}_2(t) \end{bmatrix} \\ \mathbf{d}(t) &= \begin{bmatrix} \sin(\Omega t) \mathbf{I} & \cos(\Omega t) \mathbf{I} \end{bmatrix} \begin{bmatrix} \mathbf{a}_1(t) \\ \mathbf{a}_2(t) \end{bmatrix}. \end{aligned} \quad (2)$$

Applying a similarity transformation to this system

$$\begin{aligned} \begin{bmatrix} \mathbf{a}_1(t) \\ \mathbf{a}_2(t) \end{bmatrix} &= \begin{bmatrix} \sin(\Omega t) \mathbf{I} & -\cos(\Omega t) \mathbf{I} \\ \cos(\Omega t) \mathbf{I} & \sin(\Omega t) \mathbf{I} \end{bmatrix} \begin{bmatrix} \mathbf{x}_1(t) \\ \mathbf{x}_2(t) \end{bmatrix} \\ \begin{bmatrix} \mathbf{x}_1(t) \\ \mathbf{x}_2(t) \end{bmatrix} &= \begin{bmatrix} \sin(\Omega t) \mathbf{I} & \cos(\Omega t) \mathbf{I} \\ -\cos(\Omega t) \mathbf{I} & \sin(\Omega t) \mathbf{I} \end{bmatrix} \begin{bmatrix} \mathbf{a}_1(t) \\ \mathbf{a}_2(t) \end{bmatrix} \end{aligned} \quad (3)$$

results in

$$\begin{aligned} \begin{bmatrix} \dot{\hat{\mathbf{x}}}_1(t) \\ \dot{\hat{\mathbf{x}}}_2(t) \end{bmatrix} &= \begin{bmatrix} \mathbf{0} & -\Omega \mathbf{I} \\ \Omega \mathbf{I} & \mathbf{0} \end{bmatrix} \begin{bmatrix} \hat{\mathbf{x}}_1(t) \\ \hat{\mathbf{x}}_2(t) \end{bmatrix} \\ \mathbf{d}(t) &= \begin{bmatrix} \mathbf{I} & \mathbf{0} \end{bmatrix} \begin{bmatrix} \hat{\mathbf{x}}_1(t) \\ \hat{\mathbf{x}}_2(t) \end{bmatrix}. \end{aligned} \quad (4)$$

This second state space description (4) has a constant state and output matrix for a constant rotational speed Ω and forms the basis for the stability analysis. The similarity transformation maps the signals from a static to a rotating coordinate frame — a technique that is also known as amplitude modulation/demodulation and as the park/inverse park transformation [4] in field oriented motor control algorithms.

It is easy to see that the system matrix describes harmonic oscillators with the eigenfrequency Ω and no damping.

A. Observability

The observability matrix of the state space description (4) is given by

$$\mathbf{Q} = \begin{bmatrix} \mathbf{C} \\ \mathbf{CA} \end{bmatrix} = \begin{bmatrix} \mathbf{I} & \mathbf{0} \\ \mathbf{0} & -\Omega \mathbf{I} \end{bmatrix}. \quad (5)$$

\mathbf{Q} has full rank for $\Omega \neq 0$. This tells us that the system is fully observable for $\Omega \neq 0$. The poles therefore can be freely placed except for the rotational speed $\Omega = 0$.

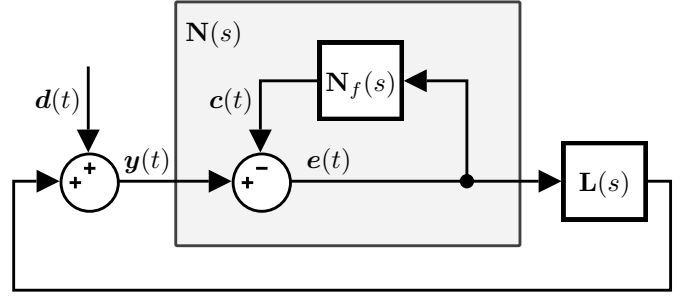


Figure 1. Block diagram of the unbalance signal $\mathbf{d}(t)$, the compensation signal $\mathbf{c}(t)$ from the observer $\mathbf{N}_f(s)$ and the loop gain $\mathbf{L}(s)$ of the inner position feedback loop.

B. Observer design

The observer based on the state space description (4) estimates the two state vectors $\mathbf{x}_1(t)$, $\mathbf{x}_2(t)$ with $\hat{\mathbf{x}}_1(t)$, $\hat{\mathbf{x}}_2(t)$. We define the error signal $\mathbf{e}(t) = \mathbf{y}(t) - \mathbf{c}(t)$ where $\mathbf{c}(t)$ is the compensation signal from the observer $\mathbf{N}_f(s)$ for the unbalance signal $\mathbf{d}(t)$. The block diagram of the closed loop system is shown in figure 1.

The error signal $\mathbf{e}(t)$ does not contain any synchronous parts anymore as soon as the observer estimate $\mathbf{c}(t)$ converged to the real unbalance response $\mathbf{d}(t)$.

Using this error signal $\mathbf{e}(t)$ as the input of the loop gain $\mathbf{L}(s)$, the error signal has also to fulfill the equation $\mathbf{e}(s) = -\mathbf{S}(s)\mathbf{c}(s)$ where $\mathbf{S}(s)$ is the output sensitivity function $\mathbf{S}(s) = (\mathbf{I} - \mathbf{L}(s))^{-1}$ of the inner control loop.

The speed dependent observer gain $\begin{bmatrix} \mathbf{T}_R(\Omega)^T & \mathbf{T}_J(\Omega)^T \end{bmatrix}^T$ weights the error signal $\mathbf{e}(t)$ and updates the observer states

$$\begin{aligned} \begin{bmatrix} \dot{\hat{\mathbf{x}}}_1(t) \\ \dot{\hat{\mathbf{x}}}_2(t) \end{bmatrix} &= \begin{bmatrix} \mathbf{0} & -\Omega \mathbf{I} \\ \Omega \mathbf{I} & \mathbf{0} \end{bmatrix} \begin{bmatrix} \hat{\mathbf{x}}_1(t) \\ \hat{\mathbf{x}}_2(t) \end{bmatrix} + \begin{bmatrix} \mathbf{T}_R(\Omega) \\ \mathbf{T}_J(\Omega) \end{bmatrix} \mathbf{e}(t) \\ \mathbf{c}(t) &= \begin{bmatrix} \mathbf{I} & \mathbf{0} \end{bmatrix} \begin{bmatrix} \hat{\mathbf{x}}_1(t) \\ \hat{\mathbf{x}}_2(t) \end{bmatrix}. \end{aligned} \quad (6)$$

The transfer function matrix from $\mathbf{e}(s)$ to $\mathbf{c}(s)$ is

$$\begin{aligned} \mathbf{N}_f(s) = \frac{\mathbf{c}(s)}{\mathbf{e}(s)} &= \begin{bmatrix} \mathbf{I} & \mathbf{0} \end{bmatrix} \begin{bmatrix} s\mathbf{I} & \Omega \mathbf{I} \\ -\Omega \mathbf{I} & s\mathbf{I} \end{bmatrix}^{-1} \begin{bmatrix} \mathbf{T}_R(\Omega) \\ \mathbf{T}_J(\Omega) \end{bmatrix} \\ &= \frac{1}{s^2 + \Omega^2} (s\mathbf{T}_R(\Omega) - \Omega \mathbf{T}_J(\Omega)). \end{aligned} \quad (7)$$

To simplify further calculations, the state matrix is transformed into modal coordinates

$$\begin{aligned} \begin{bmatrix} \mathbf{m}_1(t) \\ \mathbf{m}_2(t) \end{bmatrix} &= \begin{bmatrix} \mathbf{I} & j\mathbf{I} \\ \mathbf{I} & -j\mathbf{I} \end{bmatrix} \begin{bmatrix} \hat{\mathbf{x}}_1(t) \\ \hat{\mathbf{x}}_2(t) \end{bmatrix} \\ \begin{bmatrix} \hat{\mathbf{x}}_1(t) \\ \hat{\mathbf{x}}_2(t) \end{bmatrix} &= \frac{1}{2} \begin{bmatrix} \mathbf{I} & \mathbf{I} \\ -j\mathbf{I} & j\mathbf{I} \end{bmatrix} \begin{bmatrix} \mathbf{m}_1(t) \\ \mathbf{m}_2(t) \end{bmatrix} \end{aligned} \quad (8)$$

resulting in the new state space description in modal form

$$\begin{aligned} \begin{bmatrix} \dot{\mathbf{m}}_1(t) \\ \dot{\mathbf{m}}_2(t) \end{bmatrix} &= \begin{bmatrix} j\Omega\mathbf{I} & \mathbf{0} \\ \mathbf{0} & -j\Omega\mathbf{I} \end{bmatrix} \begin{bmatrix} \mathbf{m}_1(t) \\ \mathbf{m}_2(t) \end{bmatrix} + \begin{bmatrix} \mathbf{T}(\Omega) \\ \overline{\mathbf{T}(\Omega)} \end{bmatrix} \mathbf{e}(t) \\ \mathbf{c}(t) &= \begin{bmatrix} \frac{1}{2}\mathbf{I} & \frac{1}{2}\mathbf{I} \end{bmatrix} \begin{bmatrix} \mathbf{m}_1(t) \\ \mathbf{m}_2(t) \end{bmatrix} \end{aligned} \quad (9)$$

where $\mathbf{T}(\Omega) = \mathbf{T}_R(\Omega) + j\mathbf{T}_J(\Omega)$ and $\overline{\mathbf{T}(\Omega)} = \mathbf{T}_R(\Omega) - j\mathbf{T}_J(\Omega)$.

The sensitivity function $\mathbf{S}(s)$ has a state space description

$$\begin{aligned} \dot{\mathbf{x}}_s(t) &= \mathbf{A}_s \mathbf{x}_s(t) + \mathbf{B}_s \mathbf{c}(t) \\ \mathbf{e}(t) &= \mathbf{C}_s \mathbf{x}_s(t) + \mathbf{D}_s \mathbf{c}(t). \end{aligned} \quad (10)$$

Closing the outer loop results in the system matrix

$$\begin{aligned} \mathbf{A}(\Omega) &= \underbrace{\begin{bmatrix} j\Omega\mathbf{I} & \mathbf{0} & \mathbf{0} \\ \mathbf{0} & -j\Omega\mathbf{I} & \mathbf{0} \\ -\frac{1}{2}\mathbf{B}_s & -\frac{1}{2}\mathbf{B}_s & \mathbf{A}_s \end{bmatrix}}_{\mathbf{A}_0(\Omega)} + \\ &\quad \underbrace{\begin{bmatrix} -\frac{1}{2}\mathbf{T}(\Omega)\mathbf{D}_s & -\frac{1}{2}\mathbf{T}(\Omega)\mathbf{D}_s & \mathbf{T}(\Omega)\mathbf{C}_s \\ -\frac{1}{2}\overline{\mathbf{T}(\Omega)}\mathbf{D}_s & -\frac{1}{2}\overline{\mathbf{T}(\Omega)}\mathbf{D}_s & \overline{\mathbf{T}(\Omega)}\mathbf{C}_s \\ \mathbf{0} & \mathbf{0} & \mathbf{0} \end{bmatrix}}_{\delta\mathbf{A}(\Omega)} \end{aligned} \quad (11)$$

where $\mathbf{A}_0(\Omega)$ is the system matrix of the open loop with the multiple eigenvalues $\pm j\Omega$ from the filter and the eigenvalues from the sensitivity function $\text{eig}(\mathbf{A}_s)$. The sensitivity of these eigenvalues with respect to $\delta\mathbf{A}(\Omega)$ can be investigated using the results from appendix A. Therefore, we need the associated eigenvectors of the multiple open loop eigenvalues $\lambda = \pm j\Omega$ of the system matrix $\mathbf{A}_0(\Omega)$. Due to the chosen modal representation, it can be shown that the stacked right and left eigenvectors \mathbf{U}_0 and \mathbf{V}_0^T for the eigenvalue $\lambda_0 = j\Omega$ are

$$\mathbf{U}_0 = \begin{bmatrix} \mathbf{I} \\ \mathbf{0} \\ -\frac{1}{2}(j\Omega\mathbf{I} - \mathbf{A}_s)^{-1}\mathbf{B}_s \end{bmatrix} \quad (12)$$

$$\mathbf{V}_0^T = \begin{bmatrix} \mathbf{I} & \mathbf{0} & \mathbf{0} \end{bmatrix} \quad (13)$$

$$\mathbf{V}_0^T \mathbf{U}_0 = \mathbf{I}. \quad (14)$$

Applying this result to equation (41) gives

$$\begin{aligned} \delta\mathbf{A}(\Omega) &= \text{eig} \left((\mathbf{V}_0^T \mathbf{U}_0)^{-1} \mathbf{V}_0^T \delta\mathbf{A}(\Omega) \mathbf{U}_0 \right) \\ &= \text{eig} \left(-\frac{1}{2} \mathbf{T}(\Omega) (\mathbf{D}_s + \mathbf{C}_s (j\Omega\mathbf{I} - \mathbf{A}_s)^{-1} \mathbf{B}_s) \right) \\ &= -\frac{1}{2} \text{eig} (\mathbf{T}(\Omega) \mathbf{S}(j\Omega)). \end{aligned} \quad (15)$$

The observer gains $\mathbf{T}_R(\Omega) = \Re(\mathbf{T}(\Omega))$ and $\mathbf{T}_J(\Omega) = \Im(\mathbf{T}(\Omega))$ are now transformed to the first state space description (2) which will be used for implementation. The observer

equations become

$$\begin{aligned} \begin{bmatrix} \dot{\hat{\mathbf{a}}}_1(t) \\ \dot{\hat{\mathbf{a}}}_2(t) \end{bmatrix} &= \begin{bmatrix} \sin(\Omega t)\mathbf{I} & -\cos(\Omega t)\mathbf{I} \\ \cos(\Omega t)\mathbf{I} & \sin(\Omega t)\mathbf{I} \end{bmatrix} \begin{bmatrix} \mathbf{T}_R(\Omega) \\ \mathbf{T}_J(\Omega) \end{bmatrix} \mathbf{e}(t) \\ &= \begin{bmatrix} \mathbf{T}_R(\Omega) & -\mathbf{T}_J(\Omega) \\ \mathbf{T}_J(\Omega) & \mathbf{T}_R(\Omega) \end{bmatrix} \begin{bmatrix} \sin(\Omega t)\mathbf{I} \\ \cos(\Omega t)\mathbf{I} \end{bmatrix} \mathbf{e}(t) \end{aligned} \quad (16)$$

$$\mathbf{c}(t) = \begin{bmatrix} \sin(\Omega t)\mathbf{I} & \cos(\Omega t)\mathbf{I} \end{bmatrix} \begin{bmatrix} \hat{\mathbf{a}}_1(t) \\ \hat{\mathbf{a}}_2(t) \end{bmatrix}$$

which are the same equations as in [1].

In the SISO case equation (15) becomes

$$\delta\lambda(\Omega) = -\frac{1}{2} T(\Omega) S(j\Omega). \quad (17)$$

C. Notch filter stability

The stability of the open loop notch filter $\mathbf{N}(s)$ is investigated in the SISO case. The notch filter transfer function $N(s)$ is

$$N(s) = \frac{1}{1 + N_f(s)} = \frac{s^2 + \Omega^2}{s^2 + \Omega^2 + sT_R(\Omega) - \Omega T_J(\Omega)}. \quad (18)$$

The two poles of the filter are

$$s_{1,2}(\Omega) = -\frac{T_R(\Omega)}{2} \pm \sqrt{\left(\frac{T_R(\Omega)}{2}\right)^2 - \Omega^2 + \Omega T_J(\Omega)} \quad (19)$$

and lay in the unstable right plane when $T_R(\Omega)$ is negative. This happens, for example, when we choose

$$T(\Omega) = -2 \frac{\delta\lambda}{S(j\Omega)} \quad (20)$$

for $\delta\lambda < 0$, $\delta\lambda \in \mathbb{R}$ and the phase of the sensitivity function is bigger than 90° , which is the case for a typical sensitivity function of a mechanical system at frequencies below the closed loop rigid body modes. But this is not a restriction, because the filter poles move to the left side when closing the outer loop.

III. TUNING GUIDELINES

The design problem to stabilise the notch filter is to specify a matrix $\mathbf{T}(\Omega)$ such that the closed loop eigenvalues $\mathbf{A}(\Omega)$ are stable. This is the same as requiring $\Re(\delta\mathbf{A}(\Omega)) < 0$. Using

$$\mathbf{T}(\Omega) = 2\mathbf{\Sigma}(\Omega)\mathbf{S}(j\Omega)^{-1} \quad (21)$$

where $\mathbf{\Sigma}(\Omega)$ is a speed dependent diagonal matrix with $\Re(\mathbf{\Sigma}(\Omega)_{i,i}) > 0$, one gets

$$\delta\mathbf{A}(\Omega) = -\mathbf{\Sigma}(\Omega). \quad (22)$$

The matrix $\mathbf{\Sigma}(\Omega)$ defines the distances of the closed loop notch filter poles from the zeros. This distance corresponds to the convergency rate of filter. Choosing a higher $\mathbf{\Sigma}$ will result in a faster adaption, but also to a filter with higher bandwidth — and higher bandwidth has impact on a wider frequency range around $\mathbf{S}(j\Omega)$ resulting in a potential stability problem. Choosing a smaller $\mathbf{\Sigma}$ results in a slow adaption, but the notch filter bandwidth can become arbitrarily small so that the filter

has almost no influence on the location of the other poles — think of a pole/zero cancellation in the transfer function or a root locus plot.

With equation (21), the matrix $\mathbf{T}(\Omega)$ is typically a dense matrix depending on the rotational speed Ω . This leads to a very complex implementation of the observer gains because all elements have to be scheduled over the operating range. In many applications, the sensitivity matrix is diagonal dominant and similar in the different channels. If not, it is possible to use a static coordinate transformation to improve this property. It is then possible to use a $\mathbf{T}(\Omega)$ matrix which is diagonal, probably with a repeated value which is used for all channels. Gain scheduling becomes much easier to implement in these cases.

The remaining question for the control engineer is to have an idea how a particular $\mathbf{T}(\Omega)$ will perform.

A. Bode diagram of eigenvalue sensitivities

Using again the definition of $\delta\mathbf{\Lambda}(\Omega)$ in equation (15) a bode diagram helps to investigate the performance and the robustness of the filter. The performance is defined as the speed of convergency which can be calculated from the absolute values of $\delta\mathbf{\Lambda}(\Omega)$. The robustness is defined as the phase reserve the pole has (as seen from the zero on the imaginary axis) before it crosses the imaginary axis. Drawing a bode diagram with

$$\mathbf{G}(j\omega) = -\delta\mathbf{\Lambda}(\Omega)|_{\Omega=\omega} \quad (23)$$

the magnitude tells us how close we match the performance requirements and the phase how robust the filter is. Negating $\delta\mathbf{\Lambda}(\Omega)$ leads to a phase diagram which is 0° when the pole is located in the stable left half plane with an angle of 90° to the zero on the imaginary axis. When the phase is $\pm 90^\circ$, the pole lays on the imaginary axis, the stability boundary.

This boundary is a necessary but not sufficient condition of closed loop stability. The reason for this is that the phase of this bode diagram is independent of the selected speed of convergency — the formula (15) is only valid for sufficiently small changes in the eigenvalues.

The presented bode diagram will therefore help to select the speed ranges where the filter has to be turned off by setting $\mathbf{T}(\Omega) = 0$.

B. Bode diagram of the robustness radius

To get a sufficient condition for stability, one could use nyquist diagrams of the loop gain $\mathbf{L}_\Omega(j\omega) = \mathbf{N}_f(j\omega)\mathbf{S}(j\omega)$ for each rotational frequency. Because $\mathbf{S}(j\omega)$ and $\mathbf{N}_f(j\omega)$ have no pole in the right hand side of the complex plane, the number of encirclements of the origin of $\det(\mathbf{I} + \mathbf{L}_\Omega(j\omega))$ has to be zero. This is a little cumbersome if one has to test this curve for several rotational speeds. Therefore, the circle with the maximum radius is calculated so that the nyquist curve touches but does not enter the circle. This radius is found by calculating the infinity norm of the closed loop sensitivity function $\mathbf{S}_\Omega(j\omega) = (\mathbf{I} + \mathbf{L}_\Omega(j\omega))^{-1}$. The radius is then defined

as

$$r(\Omega) = \frac{1}{\|\mathbf{S}_\Omega(j\omega)\|_\infty} \quad (24)$$

and is only defined if $\mathbf{S}_\Omega(j\omega)$ is stable.

The limit values for the radius $r(\Omega)$ are

$$\max_{\Omega} (r(\Omega)) = 1 \quad (25)$$

$$\min_{\Omega} (r(\Omega)) = 0 \quad (26)$$

where $r(\Omega) = 1$ indicates good robustness with a phase margin of at least $\pm 60^\circ$ and a gain margin of $\frac{1}{2} \infty$ [also known from linear quadratic regulator properties) and $r(\Omega) = 0$ indicates the stability boundary. If the adaption matrix is set to $\mathbf{T}(\Omega) = \mathbf{0}$, the stability radius becomes 1.

For this stability radius it is again possible to draw a bode diagram

$$\mathbf{R}(j\omega) = r(\Omega)|_{\Omega=\omega} \quad (27)$$

Because the radius is a real value, the magnitude diagram contains all the required information. By defining a minimum stability radius one can selectively improve the adaption matrix $\mathbf{T}(\Omega)$ at certain rotational speeds and improve the switching strategy of the filter.

Typically, the robustness radius is very close to 1 but the value can significantly decrease over a small speed range close to rotor critical speeds. It is therefore vital to switch the filter adaption off and on with a speed margin to be also robust against changes in rotor dynamics such as gyroscopic effects or temperature.

Combining the necessary phase boundary from (23) and the robustness radius (24) leads to a very helpful tool that supports the control engineer in selecting a suitable adaption matrix $\mathbf{T}(\Omega)$ and a switching strategy for the filter.

IV. SIMULATION EXAMPLE

The presented tuning guidelines are applied to a simple magnetic bearing system. Only one channel is considered. The system contains an eigenfrequency at 200Hz and a negative stiffness component from the magnetic actuator. Figure 2 shows the plant transfer function.

The plant is stabilized using a controller with a PID structure. The integrator, the second order lead element and the second order low pass filter for the roll-off result in a controller of order five. Figure 3 shows the transfer function of the discrete time controller.

The resulting output sensitivity function is shown in figure 4. This sensitivity function is used to tune and analyze the closed loop stability of the notch filter.

The rigid body mode of the closed loop system is around 40Hz, which can be seen in figure 2.

A. Choosing $T(\Omega) = 2\sigma S(j\Omega)^{-1}$

When we choose $T(\Omega)$ as suggested in equation (21), we get

$$T(\Omega) = 2\sigma S(j\Omega)^{-1} \quad (28)$$

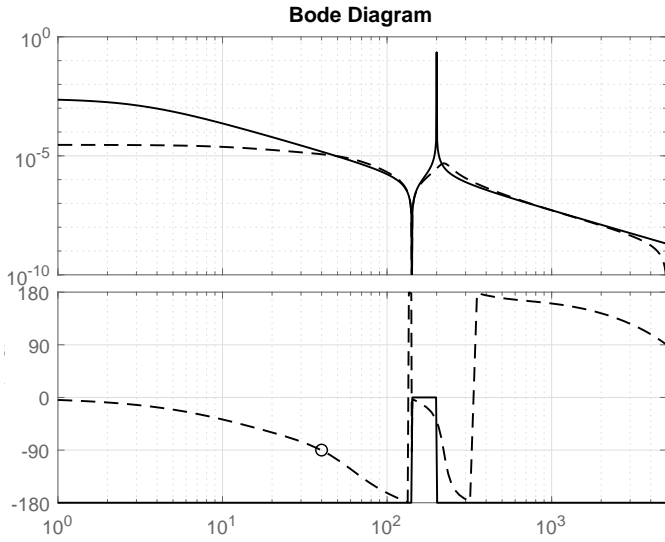


Figure 2. Magnitude of the frequency response of the plant G (solid line) and the compliance $G_f = (1 + GC)^{-1}G$ (dashed line). The circle at -90° indicates the rigid body mode frequency of the closed loop system.

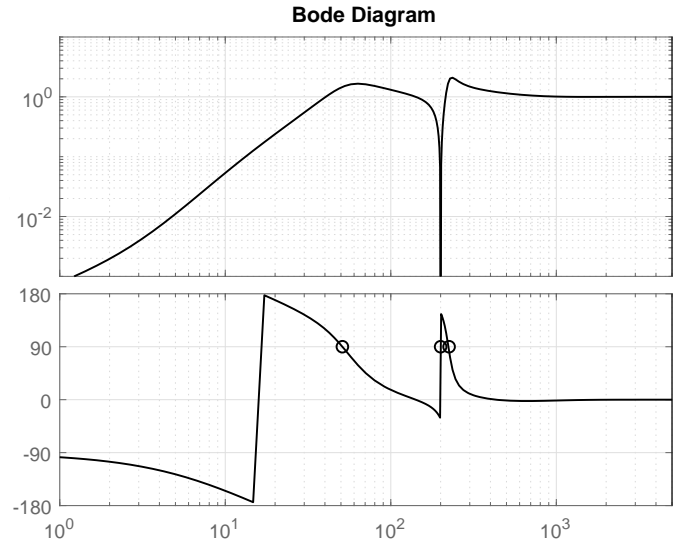


Figure 4. Output sensitivity function $S = (1 + GC)^{-1}$. The circles at 90° indicate the frequencies Ω where $T_R(\Omega) = \Re(S(j\Omega)^{-1})$ changes the sign, making the open loop notch filter unstable.

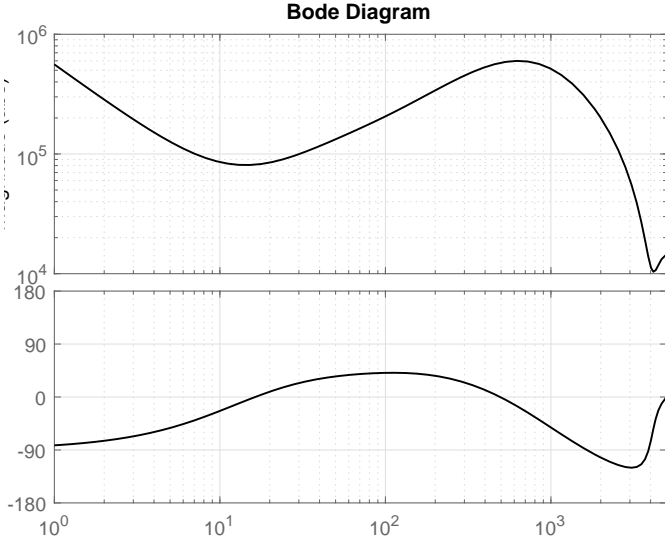


Figure 3. Controller transfer function in discrete time. The controller consists of an integrator, a second order lead element and a second order roll-off.

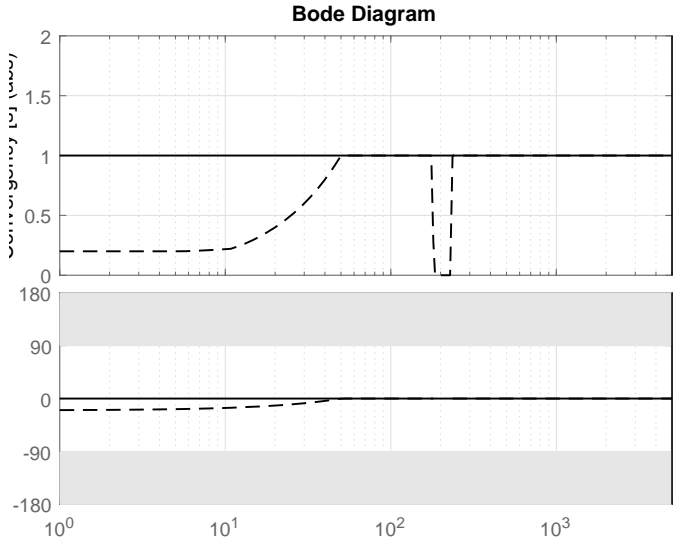


Figure 5. Bode diagram of the convergence rate and the unstable region in grey for $T(\Omega) = 2S(j\Omega)^{-1}$ (solid line) and $T(\Omega) = 2\sigma(\Omega)S(j\Omega)^{-1}$ (dashed line).

and

$$\delta\Lambda(\Omega) = -\sigma. \quad (29)$$

The bode diagram of $\delta\Lambda(\Omega)$ in figure 5 shows a constant line of magnitude σ and a constant phase of 0° . This can lead to the impression that σ can be chosen arbitrarily big without losing the stability of the closed loop. This is of course not the case, because this bode diagram is only a local analysis — it is a necessary but not sufficient stability criterion.

To investigate the stability at a certain rotational frequency, the stability radius $r(\Omega)$ is plotted in figure 6. The loop is unstable up to about 3Hz and at the eigenfrequency at 200Hz. Good filter robustness is reached above 5Hz where the robustness radius is $r(\Omega) > 0.5$.

Because $\mathbf{T}(\Omega)$ depends anyway on the rotational frequency, the convergency rate $\sigma(\Omega)$ can also be selected speed depen-

dent. Choosing a smaller $|\sigma(\Omega)|$ at speeds where the robustness radius is small can improve the filter properties. Also the phase $\arg(\sigma(\Omega))$ can be used to increase the stability radius at low speeds because at these frequencies the two poles of the filter $j\Omega$ and $-j\Omega$ interact with each other so that the eigenvalue sensitivity analysis is inaccurate. Figures 5 and 6 show also the two bode diagrams for a tuned $\sigma(\Omega)$

$$\sigma(\Omega) = \begin{cases} 0.2e^{(\frac{20^\circ}{50\text{Hz}}\Omega - 20^\circ)j} & \Omega \leq 10\text{Hz} \\ \frac{\Omega}{50\text{Hz}}e^{(\frac{20^\circ}{50\text{Hz}}\Omega - 20^\circ)j} & 10\text{Hz} < \Omega \leq 50\text{Hz} \\ 0 & 180\text{Hz} < \Omega \leq 230\text{Hz} \\ 1 & \text{otherwise} \end{cases} \quad (30)$$

with a significantly improved robustness at low speeds. Activating the filter at these low speeds does not depend anymore

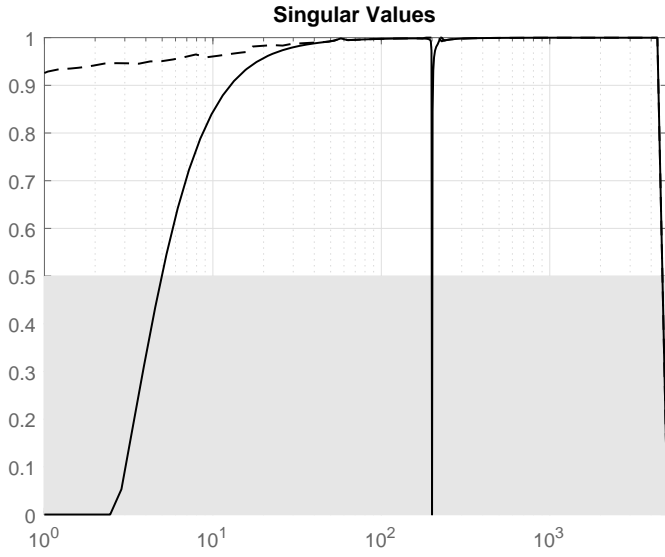


Figure 6. Stability radius $r(\Omega)$ for $T(\Omega) = 2S(j\Omega)^{-1}$ (solid line) and $T(\Omega) = 2\sigma(\Omega)S(j\Omega)^{-1}$ (dashed line).

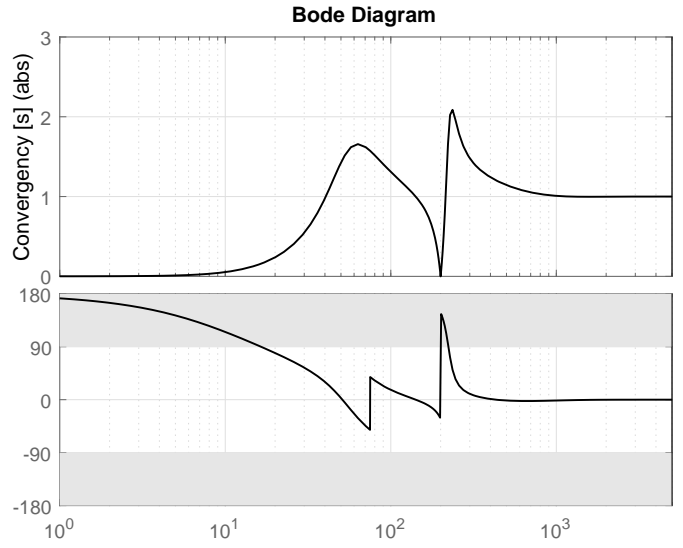


Figure 8. Bode diagram of the convergency rate and the unstable region in grey for $T(\Omega) = -2j$ for $\Omega < 75\text{Hz}$ and $T(\Omega) = 2$ for $\Omega > 75\text{Hz}$.

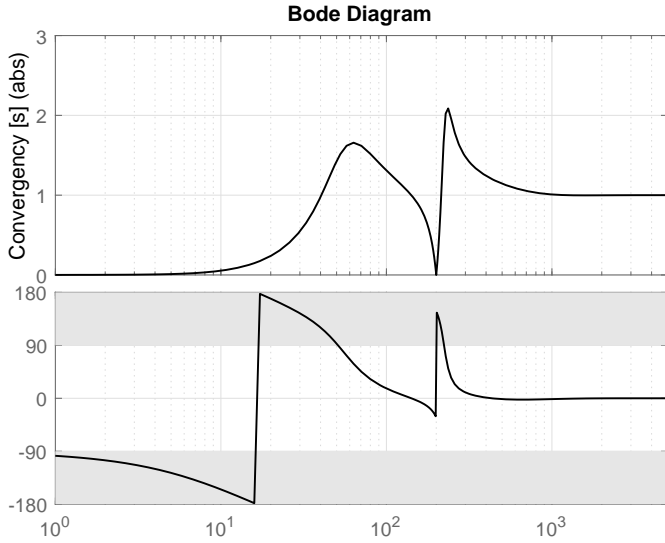


Figure 7. Bode diagram of the convergency rate and the unstable region in grey for $T(\Omega) = 2$.

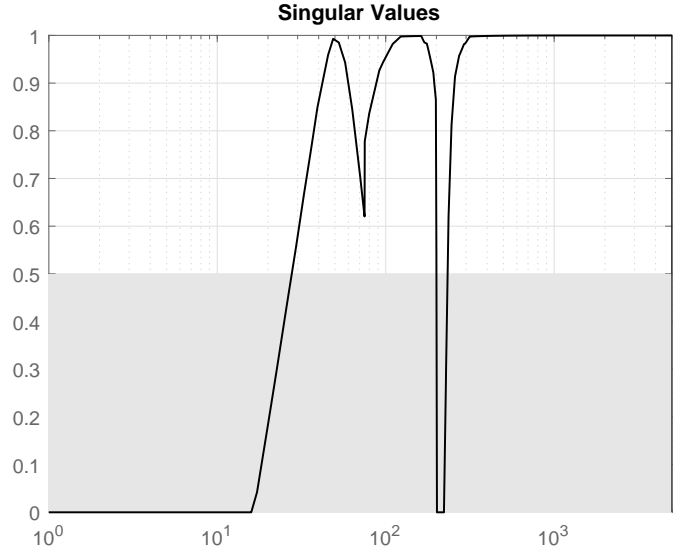


Figure 9. Stability radius $r(\Omega)$ for $T(\Omega) = -2j$ for $\Omega < 75\text{Hz}$ and $T(\Omega) = 2$ for $\Omega > 75\text{Hz}$.

on the stability of the filter but on properties of the whole system, e.g. minimum desired rate of convergency¹, external disturbances like magnetic pull of a synchronous motor, speed detection and rotor angle estimation².

B. Choosing $T(\Omega) = 2c(\Omega)$

The simplest case that can be implemented is a constant adaption matrix $T(\Omega) = 2c$. This will lead to a very straight forward implementation without gain scheduling of T . Figure 7 shows the effect of this implementation using $c = 1$ — the convergency rate of the filter depends heavily on the rotational

¹A speed of convergency of 0.2 corresponds to a time constant of 5s which is already impractical slow.

²The speed and angle information for systems with one pulse per revolution is very inaccurate at low speeds.

speed, and the filter is not stable below the rigid body mode and around the first bending mode. From this information, the unbalance compensation can be turned on above 50Hz and has to be frozen between 180Hz and 230Hz.

A simple improvement can be made by adding one switching point where the filter changes from a low speed to a high speed adaption parameter. According to figure 7 a switching point at 75Hz seems to be a good compromise resulting in a bigger stability region down to 20Hz as can be seen in figure 8 and 9. Around the bending mode, it is still necessary to freeze the adaption.

C. Other choices for $\mathbf{T}(\Omega)$

There are a lot of other choices for $\mathbf{T}(\Omega)$. Each choice will have its benefits when it comes to the implementation on a target system. Computational power, memory requirements,

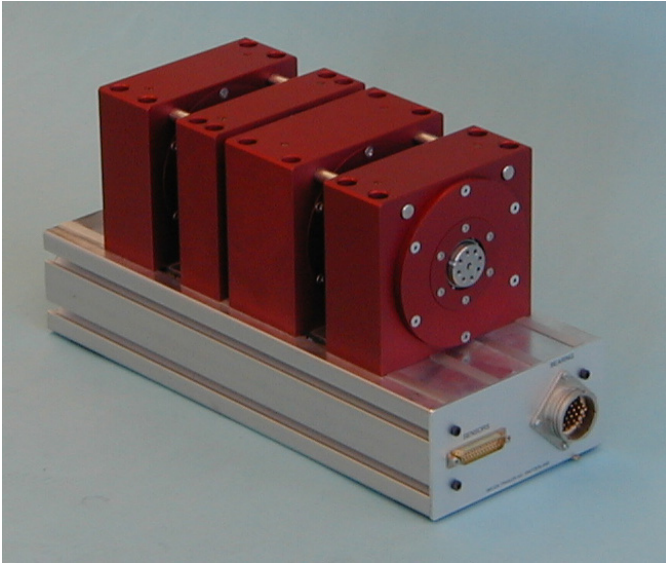


Figure 10. 5-axis test system with a flexible rotor. Rotor mass is 2.1kg.

implementation complexity but also robustness varies between all these choices. As a rule of thumb one can say that simple adaption matrices will result in simple implementations but decrease the robustness of the filter.

- $\mathbf{T}(\Omega) = -\mathbf{K}(\Omega) \arg(\mathbf{S}(j\Omega))$: Use only the phase information of the sensitivity function. The adaption speed is chosen from the control system engineer by specifying the speed dependent gain matrix $\mathbf{K}(\Omega)$.
- $\mathbf{T}(\Omega) = \text{diag}(\mathbf{T}_{full}(\Omega))$: Use only the diagonal elements of a diagonal dominant $\mathbf{T}_{full}(\Omega)$.
- $t(\Omega) = \frac{1}{p} \sum_{i=1}^p \mathbf{T}(\Omega)_{ii}$: Use only one adaption parameter for all channels by averaging the diagonal elements.
- $\mathbf{T}(\Omega) = \mathbf{T}_1 \mathbf{T}_{diag}(\Omega) \mathbf{T}_2$: Decompose a dense adaption matrix into two static (not speed dependent) matrices \mathbf{T}_1 and \mathbf{T}_2 to get a diagonal dominant matrix $\mathbf{T}_{diag}(\Omega)$. Implement the decomposed adaption matrix. It is of course possible to use $\mathbf{T}_{diag}(\Omega) = t(\Omega) \mathbf{I}$ with $t(\Omega)$ from above.

V. TESTS

The proposed filter tuning and analysis tools are applied to a 5-axis test system with a flexible rotor. Figure 10 shows a picture of the system. The magnetic bearing controller is capable to schedule a dense adaption matrix $\mathbf{T}(\Omega)$ over the operating speed range.

The radial position controller is tuned with a model based design approach and therefore a MIMO controller of order 40 stabilizes the rotor. The control loop runs with 10kHz sampling frequency. The resulting eigenfrequency of the rigid body modes are about 60Hz.

Using the simplest implementation of the adaption matrix $\mathbf{T}(\Omega) = 2c\mathbf{I}$ for $c = 1$ results in the bode diagram in figure 11. The filter is unstable below a rotational frequency of about 150Hz and becomes again unstable when crossing the bending mode.

Using the equation (21) to tune $\mathbf{T}(\Omega)$ results in an improved range of stability. The convergency rate $\Sigma(\Omega)$ was selected as

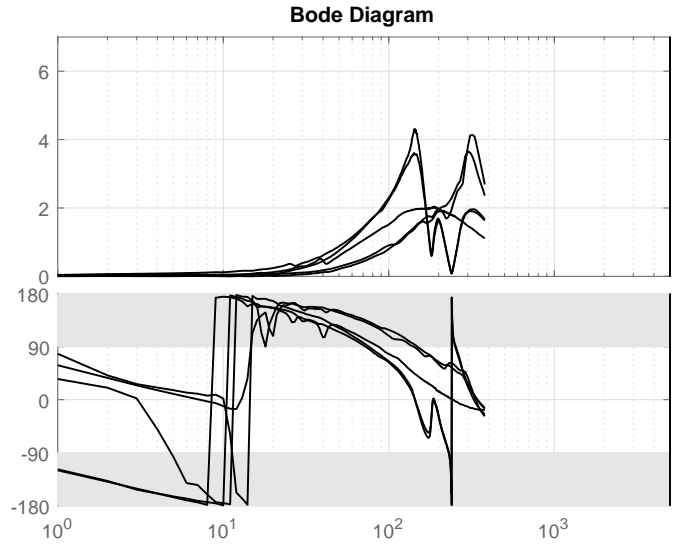


Figure 11. Bode diagram of the convergency rates and the unstable region in grey for $\mathbf{T}(\Omega) = 2\mathbf{I}$.

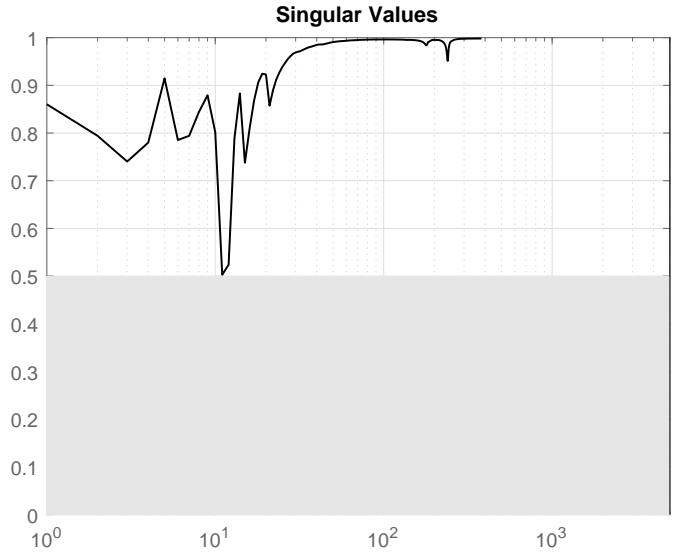


Figure 12. Stability radius $r(\Omega)$ for $\mathbf{T}(\Omega) = 2\Sigma\mathbf{S}(j\Omega)^{-1}$ with $\Sigma = \frac{1}{2}\mathbf{I}$.

$\Sigma = \sigma\mathbf{I}$ with $\sigma = 0.5$. This selection will result in a settling time of the filter of $t_{63\%} = \frac{1}{\sigma} = 2\text{s}$ for all channels. The output sensitivity function $\mathbf{S}(j\omega)$ was measured at standstill. The resulting stability radius plot is shown in figure 12. From this graph one can see that the predicted stability of the notch filter is good over the whole speed range.

To test the robustness of the filter on the real system, the rotor is held at a rotational speed of 15Hz. According to figure 12 the robustness radius is about 0.9. This indicates a good stability reserve. To test the robustness and performance of the filter, one of the integrator states \hat{a} is excited by adding an offset of $10\mu\text{m}$ while all 10 integrator states (two per axis) are measured. A good robustness is achieved when the response is similar to a step response of a first order system and only the excited integrator shows a major reaction — this indicates a good decoupling of the different channels. The time the

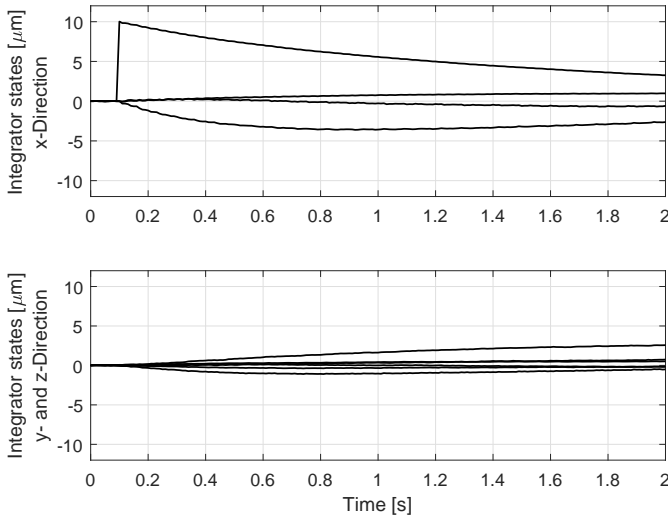


Figure 13. Step responses of an integrator excitation of $10\mu\text{m}$ at a speed of 15Hz of the test rig. The initial values of the integrator states were subtracted.

integrator state needs to converge back to the steady state value gives an information about the performance which was specified by σ . Figure 13 shows the step responses separated in x - and y/z -direction. The integrator for the cosine amplitude of the second bearing is excited. The reaction is clearly visible in the figure. The convergency rate corresponds nicely to the selected 2s . The integrator of the cosine amplitude of the first bearing shows also a significant reaction — it seems that the decoupling of the two bearings in the adaption matrix is not optimal. All the other reactions are small, but they are present. This was to be expected due to the slightly reduced stability radius.

This excitation test is very useful to investigate the filter robustness and performance at different rotational speeds and can be easily included in a standard measurement set during commissioning of a rotor.

VI. IMPLEMENTATION ASPECTS

A. Discrete state space representation

The state space description (16) is used to implement the observer because the state matrix does not depend on Ω . Using the euler method, the discrete form of the observer is

$$\begin{aligned} \begin{bmatrix} \hat{\mathbf{a}}_{1k+1} \\ \hat{\mathbf{a}}_{2k+1} \end{bmatrix} &= \begin{bmatrix} \hat{\mathbf{a}}_{1k} \\ \hat{\mathbf{a}}_{2k} \end{bmatrix} + \\ &t_s \begin{bmatrix} \mathbf{T}_R(\Omega) & -\mathbf{T}_J(\Omega) \\ \mathbf{T}_J(\Omega) & \mathbf{T}_R(\Omega) \end{bmatrix} \begin{bmatrix} \sin(\Omega t_k) \mathbf{I} \\ \cos(\Omega t_k) \mathbf{I} \end{bmatrix} e_k \quad (31) \\ \mathbf{c}_k &= \begin{bmatrix} \sin(\Omega t_k) \mathbf{I} & \cos(\Omega t_k) \mathbf{I} \end{bmatrix} \begin{bmatrix} \hat{\mathbf{a}}_{1k} \\ \hat{\mathbf{a}}_{2k} \end{bmatrix} \end{aligned}$$

where t_s is the sampling interval and $t_k = kt_s$. The sampling interval t_s can be included in the parameter $\mathbf{T}(\Omega)$ to save some multiplication instructions.

A second argument for this implementation is the stability of this filter. The euler method will map the poles at the origin to

1, transforming integrators to accumulators. Applying the euler method to the description (4) will lead to unstable discrete poles lying outside the unit circle.

A third argument for this implementation are the states $\hat{\mathbf{a}}_{1k}$, $\hat{\mathbf{a}}_{2k}$ which represent directly the amplitudes of the unbalance. These amplitudes are constant because the unbalance response itself has constant amplitudes for a given rotational speed Ω . The state space description (4) has the same I/O behaviour but the states change sinusoidally with the frequency Ω for a constant unbalance. This can lead to numerical problems in the implementation.

B. Smooth switching

An additional important point is that the matrix $\mathbf{T}(\Omega)$ is used to build the *input* matrix of the filter. Using this input matrix itself as a similarity transformation, one can also think of an implementation where $\mathbf{T}(\Omega)$ is used to build the *output* matrix of the filter and the input matrix is a unitary matrix. The I/O behaviour will be the same but the meaning of the states will change. When $\mathbf{T}(\Omega)$ is not smooth, the compensation signal $c(t)$ will contain transients whenever $\mathbf{T}(\Omega)$ changes under rotation because the filter states will converge to different values.

The authors of [5] chose discrete switching points to change between different constant adaption matrices — and because the adaption was applied at the output of the filter, a smoothing strategy was necessary. Such kind of smoothing can be avoided when the adaption matrix is used as the input of the notch filter.

C. Discrete simulation

To simulate the discrete time closed loop system at a certain rotational speed, the system description (31) is transformed using the similarity transformation (3), resulting in the state space description

$$\begin{aligned} \begin{bmatrix} \hat{\mathbf{x}}_{1k+1} \\ \hat{\mathbf{x}}_{2k+1} \end{bmatrix} &= \begin{bmatrix} \cos(\Omega t_s) \mathbf{I} & -\sin(\Omega t_s) \mathbf{I} \\ \sin(\Omega t_s) \mathbf{I} & \cos(\Omega t_s) \mathbf{I} \end{bmatrix} \begin{bmatrix} \hat{\mathbf{x}}_{1k} \\ \hat{\mathbf{x}}_{2k} \end{bmatrix} + \\ &t_s \begin{bmatrix} \cos(\Omega t_s) \mathbf{I} & -\sin(\Omega t_s) \mathbf{I} \\ \sin(\Omega t_s) \mathbf{I} & \cos(\Omega t_s) \mathbf{I} \end{bmatrix} \begin{bmatrix} \mathbf{T}_R(\Omega) \\ \mathbf{T}_J(\Omega) \end{bmatrix} e_k \quad (32) \\ \mathbf{c}_k &= \begin{bmatrix} \mathbf{I} & \mathbf{0} \end{bmatrix} \begin{bmatrix} \hat{\mathbf{x}}_{1k} \\ \hat{\mathbf{x}}_{2k} \end{bmatrix}. \end{aligned}$$

This description has constant matrices for a constant rotational speed Ω . It corresponds to the discrete approximation of the state space description (4) using the impulse invariant method [6].

VII. CONCLUSION

The generalized notch filter stability has been shown by using a sensitivity analysis of the eigenvalues of the notch filter when closing the control loop.

From this result, different possibilities of selecting the adaption matrix $\mathbf{T}(\Omega)$ are shown and their effect on robustness and performance was analyzed with the help of bode diagrams

of the eigenvalue sensitivity $\delta\Lambda(\Omega)$ and a robustness radius $r(\Omega)$.

A simple example with one channel has verified the usefulness of the bode diagrams to investigate the filter stability, tune the convergency rates and select the speed ranges where the notch filter is active.

The tuning was successfully applied to a 5-axis test system. It was shown that a well tuned filter is capable of being activated well below the rigid body modes.

Eventually some implementation and simulation aspects have been presented.

APPENDIX

A. Sensitivity of multiple eigenvalues

The following derivation of the sensitivity of eigenvalues of a matrix is based on [7] and [8].

Given is a symmetric matrix \mathbf{A}_0 with an eigenvalue λ_0 with multiplicity m and the corresponding right eigenvectors $\mathbf{U}_0 = [\mathbf{u}_0^1 \ \mathbf{u}_0^2 \ \dots \ \mathbf{u}_0^m]$ and left eigenvectors $\mathbf{V}_0 = [\mathbf{v}_0^1 \ \mathbf{v}_0^2 \ \dots \ \mathbf{v}_0^m]$. The eigenvalue equations are

$$\mathbf{A}_0 \mathbf{U}_0 = \lambda_0 \mathbf{U}_0 \quad (33)$$

$$\mathbf{V}_0^T \mathbf{A}_0 = \lambda_0 \mathbf{V}_0^T. \quad (34)$$

Now we define a perturbed matrix \mathbf{A} with perturbed eigenvalues Λ and perturbed right eigenvectors \mathbf{U} ³

$$\mathbf{A} = \mathbf{A}_0 + \delta\mathbf{A} \quad (35)$$

$$\Lambda = \lambda_0 \mathbf{I} + \delta\Lambda \quad (36)$$

$$\mathbf{U} = \mathbf{U}_0 \mathbf{X} \quad (37)$$

where $\delta\mathbf{A}$ is a known perturbation. $\delta\Lambda$ is a diagonal matrix expressing the sensitivity of the eigenvalues $\lambda_0 \mathbf{I}$. \mathbf{X} is a matrix of full rank m . The eigenvalue equation of the perturbed matrix is

$$\mathbf{A}\mathbf{U} = \mathbf{U}\Lambda. \quad (38)$$

Using (35) - (37) gives

$$(\mathbf{A}_0 + \delta\mathbf{A})\mathbf{U}_0 \mathbf{X} = \mathbf{U}_0 \mathbf{X} (\lambda_0 \mathbf{I} + \delta\Lambda). \quad (39)$$

Expanding and multiplying with \mathbf{V}_0^T from the left gives

$$\begin{aligned} \mathbf{V}_0^T \delta\mathbf{A} \mathbf{U}_0 \mathbf{X} &= \mathbf{V}_0^T \mathbf{U}_0 \mathbf{X} \delta\Lambda \\ \Rightarrow (\mathbf{V}_0^T \mathbf{U}_0)^{-1} \mathbf{V}_0^T \delta\mathbf{A} \mathbf{U}_0 \mathbf{X} &= \mathbf{X} \delta\Lambda \end{aligned} \quad (40)$$

which is again an eigenvalue equation with the eigenvalues $\delta\Lambda$ and the right eigenvectors \mathbf{X} . It follows that

$$\delta\Lambda = \text{eig}((\mathbf{V}_0^T \mathbf{U}_0)^{-1} \mathbf{V}_0^T \delta\mathbf{A} \mathbf{U}_0) \quad (41)$$

which means that the eigenvalue sensitivity $\delta\Lambda$ can be expressed by the unperturbed eigenvectors \mathbf{U}_0 , \mathbf{V}_0 and the perturbation $\delta\mathbf{A}$.

³The same result is obtained when defining $\mathbf{U} = (\mathbf{U}_0 + \delta\mathbf{U})\mathbf{X}$ and neglecting products of δ -terms of higher order.

REFERENCES

- [1] R. Herzog, P. Bühler, C. Gähler, and R. Larsonneur, "Unbalance compensation using generalized notch filters in the multivariable feedback of magnetic bearings," *IEEE Transactions on control systems technology*, vol. 4, no. 5, pp. 580–586, 1996.
- [2] D. G. Luenberger, "Observing the state of a linear system," *IEEE transactions on military electronics*, vol. 8, no. 2, pp. 74–80, 1964.
- [3] H. Bleuler, M. Cole, P. Keogh, R. Larsonneur, E. Maslen, Y. Okada, G. Schweitzer, A. Traxler *et al.*, *Magnetic bearings: theory, design, and application to rotating machinery*. Springer Science & Business Media, 2009.
- [4] R. H. Park, "Two-reaction theory of synchronous machines generalized method of analysis-part i," *Transactions of the American Institute of Electrical Engineers*, vol. 48, no. 3, pp. 716–727, 1929.
- [5] K. Zhang, J. Yin, and X. Dai, "A smooth switch between different unbalance control parameters in rotor systems with active magnetic bearings," *Proceedings of ISMB15*, pp. 365–372, 2016.
- [6] J. I. Smith, "Impulse invariant method," *Physical Audio Signal Processing*, 2007.
- [7] P. Lancaster, "On eigenvalues of matrices dependent on a parameter," *Numer. Math.*, vol. 6, no. 1, pp. 377–387, Dec. 1964. [Online]. Available: <http://dx.doi.org/10.1007/BF01386087>
- [8] Wikipedia, "Eigenvalue perturbation — Wikipedia, the free encyclopedia," 2018. [Online]. Available: https://en.wikipedia.org/wiki/Eigenvalue_perturbation